Nuclear Physics A530 (1991) 211–231
North-Holland

# THE LEVEL STRUCTURE OF $^{87}$Nb

B.J. MIN[1], S. SUEMATSU, S. MITARAI and T. KUROYANAGI

*Department of Physics, Faculty of Science, Kyushu University, Fukuoka 812, Japan*

K. HEIGUCHI

*Graduate School of Science and Technology, Niigata University, Niigata 950-21, Japan*

M. MATSUZAKI[2]

*Institute of Physics, University of Tsukuba, Ibaraki 305, Japan*

Received 26 October 1990
(Revised 28 January 1991)

**Abstract:** The level structure of $^{87}$Nb has been studied through $\beta$-decay of $^{87}$Mo activity produced by the $^{58}$Ni($^{32}$S, 2pn) reaction and through in-beam $\gamma$-ray measurements in the $^{58}$Ni($^{32}$S, 3p$\gamma$)$^{87}$Nb reaction. In the $\beta$-decay study, the decay scheme of $^{87}$Mo is constructed firstly from $\gamma$-ray energies, intensities of $\gamma$-rays and conversion electrons, and $\gamma\gamma$-, $\beta\gamma$- and $\gamma$(ce)-coincidence relations. Spins and parities of the low-lying states of $^{87}$Nb and $^{87}$Zr were also investigated. In the in-beam study, intensities, coincidence relations and angular distributions of $\gamma$-rays were measured in coincidence with charged particles evaporated from the compound nuclei. Then high-spin states of $J^{\pi} \leqslant (\frac{33}{2}^{+})$ in $^{87}$Nb were established in this study. Systematic behavior in the level structures of $N = 46$ isotones, and the comparison between those of $^{85}$Y and $^{87}$Nb, are discussed.

E

RADIOACTIVITY $^{87}$Mo [from $^{58}$Ni($^{32}$S, n2p)]; $^{87,87m}$Nb [from $^{58}$Ni($^{32}$S, 3p), $E$ = 105 MeV]; measured $E_\gamma$, $I_\gamma$, $T_{1/2}$, $I$(ce). $^{87}$Nb deduced levels, $J$, $\pi$. Enriched target, Si(Au) detector, intrinsic and GAMMA-X Ge detectors, plastic scintillator.

NUCLEAR REACTIONS $^{58}$Ni($^{32}$S, 3p), $E$ = 103 MeV; measured $E_\gamma$, $I_\gamma$, $I_\gamma(\theta)$, $(xp\gamma\alpha)\gamma$-, and (2p+3p) $\gamma\gamma$-coin. $^{87}$Nb deduced levels, $J$, $\pi$, $\delta$. Enriched target, Ge, S: detectors.

## 1. Introduction

Recent studies have revealed many interesting features of the neutron deficient nuclei in $A = 80 \sim 90$ mass region. Nuclei of $N = 50$ and 48 appear to be spherical, while $N = 42$ nuclei appear to be well deformed. Previously studied $N = 46$ and 44 nuclei, which lie between these extremes, have shown both vibrational and rotational characters. Behavior of the yrast line of $N = 46$ nuclei exhibits characters of shape transitions. Thus it is of interest to study the level structure of $^{87}$Nb which is one of $N = 46$ nuclei.

Decay schemes [1-3]) of an isomeric pair ($\frac{1}{2}^{-}$ and $\frac{9}{2}^{+}$) in $^{87}$Nb have been proposed. However, the spins and parities of this isomeric pair have not been established and

[1] Present address: Design Analysis Department, Korea Atomic Energy Research Institute P.O. Box 7, Daeduk-danji, Daejeon 305-353, Korea.

[2] Present address: Department of Physics, Fukuoka University of Education, 729 Akama, Munakata city, Fukuoka 811-41, Japan.

it is undefinable which state of the pair is a ground state. Only two gamma rays (263 and 397 keV) following the decay of $^{87}$Mo produced by the $^{58}$Ni($^{32}$S, 2pn) reaction have been reported by Korschinek *et al.* [2]), Della Negra *et al.* [3]) and Hagberg *et al.* [4]). The half-life (15 ± 2 s) and $Q_{EC}$ value (6.38 ± 0.31 MeV) of the $\beta^+$ decay of $^{87}$Mo have been also reported in these works. But decay scheme of $^{87}$Mo from $\beta$-decay measurement and level scheme of $^{87}$Nb from in-beam experiment have not been reported yet.

In the present work, the low-spin states in $^{87}$Nb were investigated through the $\beta$-decay of $^{87}$Mo which is produced by the $^{58}$Ni($^{32}$S, 2pn) reaction at 105 MeV. Moreover, the high-spin states of $^{87}$Nb, which is produced by the $^{58}$Ni($^{32}$S, 3p) reaction at 103 MeV, were studied by in-beam spectroscopy.

In this paper, the new level scheme of $^{87}$Nb is reported and discussed about systematic change of nuclear structure in this region and comparison of the band structures of $^{87}$Nb and $^{85}$Y [ref. [5])].

## 2. Experimental procedures

### 2.1. BETA-GAMMA STUDY

The radioactive isotopes of $^{87}$Mo and $^{87}$Nb were produced by the $^{58}$Ni($^{32}$S, 2pn)$^{87}$Mo and $^{58}$Ni($^{32}$S, 3p)$^{87}$Nb reactions, respectively. The 105 MeV $^{32}$S beam was supplied by Kyushu University tandem electrostatic accelerator. Targets of 1.4 and 1.7 mg/cm$^2$ thickness were prepared by electroplating enriched $^{58}$Ni material (99.76%) on 2 mg/cm$^2$ gold foils.

A rotating disk isotope-transport system [6]) was used to observe decay of the isotopes. The system consists of an aluminum vacuum chamber, a stepping motor and a 0.1 mm thick aluminum rotating disk, which is 22 cm in diameter. The target was mounted at 2.5 mm in front of the disk. The reaction products are implanted in gold foils attached to the disk. Then the activities are transported to a counting position within 0.15 s by 90° rotation of the disk. Gamma, $\beta$- and X-rays, and internal conversion electrons were measured at the counting position. Operation of the system was controlled by a microcomputer.

Gamma rays from the activities implanted in the disk were detected through the aluminum window of 0.3 mm thickness by an intrinsic Ge detector of 1.9 keV resolution (FWHM) at 1.33 MeV and 16.7% relative efficiency. The detector was placed at 5.5 mm from the disk. Energy and efficiency calibrations were carried out with standard sources of $^{60}$Co, $^{57}$Co, $^{137}$Cs and $^{22}$Na.

Internal conversion electrons were measured by an 1.2 mm thick Si(Au) detector of 2.0 keV resolution (FWHM) for 59.54 keV $\gamma$-ray. This detector was placed at 10 mm in front of the rotating disk and operated in the vacuum chamber. In order to determine the internal conversion coefficients of various transitions in $^{87}$Nb and

$^{87}$Zr, the $\gamma$-rays and the internal conversion electrons were measured simultaneously. The efficiency of the Si(Au) detector was calibrated by measuring internal conversion electrons from a $^{137}$Cs source.

In $\gamma\gamma$-coincidence measurement, the intrinsic Ge detector and a GAMMA-X Ge detector were placed on each side of the disk at the same distance of 12 mm. The GAMMA-X Ge detector has 1.9 keV resolution (FWHM) at 1.33 MeV and 18% relative efficiency. To measure low-energy radiations, a 0.03 mm thick aluminum foil was used for the vacuum-chamber window. Energy signals from the detectors and time-interval signals from a time-to-amplitude converter were recorded with detected times of coincident events in 4-dimensional list mode. About 1.46 million events were accumulated and subsequently analyzed off line.

In $\beta\gamma$-coincidence measurement, the intrinsic Ge detector was replaced by a 52 mm × 60 mm plastic scintillation detector. Energy loss of positrons in the window was less than the experimental uncertainty, and was thus neglected in the analysis.

### 2.2. IN-BEAM STUDY

The levels in $^{87}$Nb were populated in the $^{58}$Ni($^{32}$S, 3p$\gamma$)$^{87}$Nb reaction at the bombarding energy of 103 MeV. A target of 10 mg/cm$^2$ was made by electroplating $^{58}$Ni material enriched to 99.76% on a gold foil of 20 mg/cm$^2$. Although $\gamma$-ray spectrum from the $^{58}$Ni + $^{32}$S reaction is complex, gamma rays from $^{87}$Nb were identified by (charged particles) $\gamma$-coincidence technique which makes it possible to determine the charged-particle multiplicity.

An array of charged-particle detectors, named Si Ball [7]) was used for the particle-$\gamma$-coincidence measurements. Si Ball consists of 11 ion-implanted Si detectors. Each Si detector has a pentagonal shape and is divided into two parts. The Si Ball can thus be operated as an 11 or an 11 × 2 detector array. The Si detectors (170 μm thickness) were arranged on a dodecahedron and the target was mounted at the center of the dodecahedron. This arrangement of the individual detectors constitutes the Si Ball which works as a very efficient multiplicity filter for protons and alpha particles. A drawing of the Si Ball is shown in fig. 1.

In the present measurement, 17 (out of 22) detector elements of Si Ball were used: six detectors in front side of the target in two-segment mode and the rest in one-segment. Each of the 17 detectors had nearly the same counting rate. The total efficiency of Si Ball was estimated to be 68% and 38% for evaporated protons and alpha particles, respectively. Loss of efficiency is mainly due to attenuation in the target, target backing and target holder.

The thickness of the target and gold backing were chosen to stop projectiles and reaction products but pass the protons and the alpha particles from the fusion reaction. The GAMMA-X Ge detector was placed at 90° to the beam direction and at a distance of 9 cm from the target. Data were accumulated in list mode, and subsequently analyzed off line.

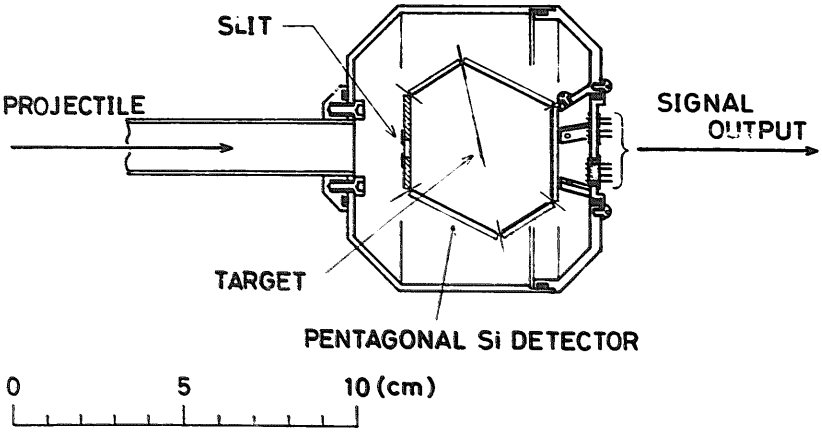


Fig. 1. The cross-sectional view of the Si Ball system which is used to measure the charged-particle multiplicity.

Angular distributions of the $\gamma$-rays were measured to determine the multipolarities. To obtain pure spectra of $\gamma$-rays from $^{87}$Nb, it was necessary to gate with three evaporated protons. Another GAMMA-X Ge detector with 1.95 keV resolution (FWHM) for the 1.33 MeV $\gamma$-ray and 20% relative efficiency was placed at a distance of 10 cm from the target and moved at 10°, 30°, 45°, 60° and 90° to the beam direction. The GAMMA-X Ge detector mentioned before was kept at 270° to the beam direction for normalization.

In order to obtain cascade relations of the $\gamma$-rays from the excited states of $^{87}$Nb, (charged particle) $\gamma\gamma$-coincidence experiment were carried out using two GAMMA-X Ge detectors and Si Ball.

## 3. Results

### 3.1. THE DECAY STUDY OF $^{87}$Mo

*3.1.1. Assignment of $\gamma$-rays.* Gamma rays following the decay of $^{87}$Mo produced through the $^{58}$Ni($^{32}$S, 2pn) reaction were measured in singles and $\beta\gamma$-coincidence. The $\gamma$-ray spectrum projected from $\beta\gamma$-coincidence matrix is shown in fig. 2. The coincidence matrix results from many cycles of 10 s irradiation and 40 s counting.

The 201.0 and 471.0 keV $\gamma$-rays shown in fig. 2 have been previously assigned to the $\beta$-decay of $^{87}$Nb [refs. [1-3,8])]. The 436.0 keV $\gamma$-ray was assigned to the $\beta$-decay of $^{42m}$Sc, which was produced by $^{32}$S+$^{12}$C (carbon is a contaminant in the target). Only two $\gamma$-rays of 263.0 and 396.8 keV have been assigned previously to the $\beta$-decay of $^{87}$Mo [refs. [2,3])].

From analyses of decay curves of these $\gamma$-rays, the half-life of $^{87}$Mo was determined to be 14.5 ± 0.3 s, which agrees with previous results [15 ± 2 s, see refs. [2-4])]. A half-life of 133.9 keV $\gamma$-ray was determined to be 14.2 ± 1.0 s. From this value, it seems that the $\gamma$-ray is fed by decay of $^{87}$Mo. Since intensity was very weak, the half-life of 334.0 keV $\gamma$-ray was not determined.

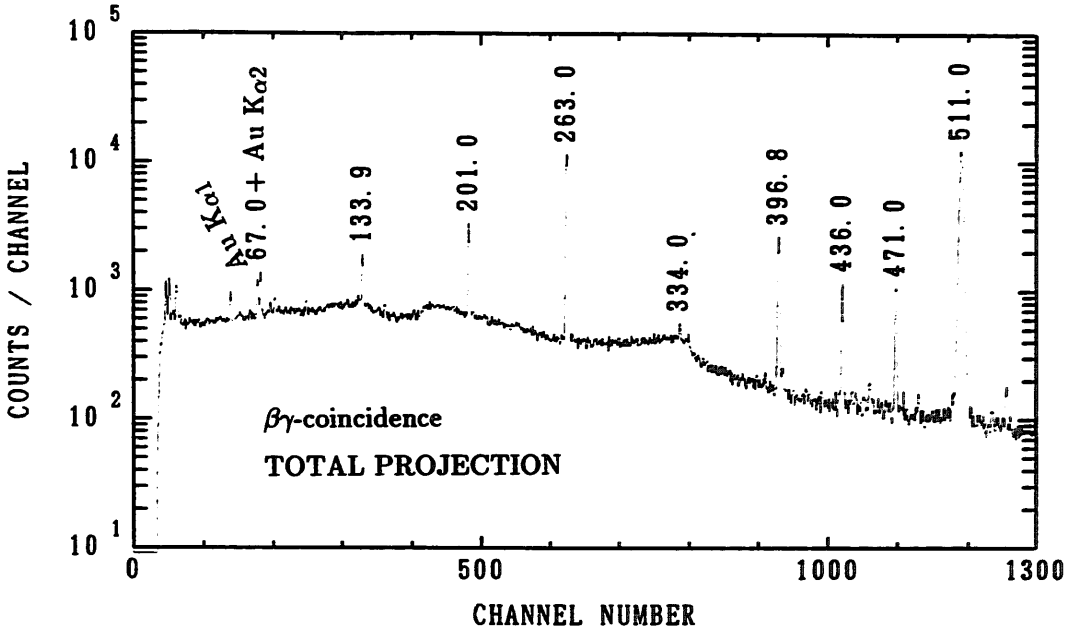


Fig. 2. Projected spectrum of γ-rays obtained from β γ-coincidence measurement in which activities were produced by $^{58}$Ni+$^{32}$S (105 MeV) reaction. The irradiation and measurement times were 10 and 40 s, respectively. Peaks are labelled by their energies in keV.

Presently, the observed intensity ratio of $K_{\alpha 1}$ (68.80 keV) and $K_{\alpha 2}$ (66.99 keV) X-rays of Au, which is the catcher material of the rotating disk, was not consistent with the established value [9]. This inconsistency may be due to the presence of the 67.0 keV γ-ray overlapped with the $K_{\alpha 2}$ X-ray. The presence of the 67.0 keV γ-ray was shown in γγ-coincidence measurement.

*3.1.2. γγ- and βγ-coincidence measurements.* In the γγ-coincidence measurement, the irradiation and counting times were 10 and 30 s, respectively. A coincidence spectrum gated by the 263.0 keV γ-ray is shown in fig. 3. The 67.0 and 133.9 keV γ-rays appear in the spectrum, thus they are assigned to the $^{87}$Mo decay. However, no γ-rays were observed in coincidence with the 396.8 keV γ-ray.

The end-point energy of positrons following the decay of $^{87}$Mo was deduced from the analysis of a positron spectrum measured in coincidence with the 263.0 keV γ-ray. Beta-energy calibrations were carried out using the $^{83}$Zr, $^{83}$Y and $^{82}$Y sources [10]. The end-point energy of the positrons in coincidence with the 263.0 keV γ-ray was determined to be 5.3 ± 0.3 MeV, which deduced a $Q_{EC}$ value of 6.6 ± 0.3 MeV for $^{87}$Mo. This $Q_{EC}$ value is in agreement with the previous result, $Q_{EC}$ = 6.38 ± 0.31 MeV [ref. [3])], within the experimental uncertainty.

To obtain absolute intensities of the γ-rays following the decay of $^{87}$Mo, intensity ratios of the γ-rays to the annihilation radiations were measured. The irradiation and measurement times of 30 and 400 s, respectively, were selected and the activities were covered by aluminum stopper with 14 mm thickness to stop all positrons [11]. Thus the γ-ray intensities via the decay of $^{87}$Mo were determined. Energies, relative

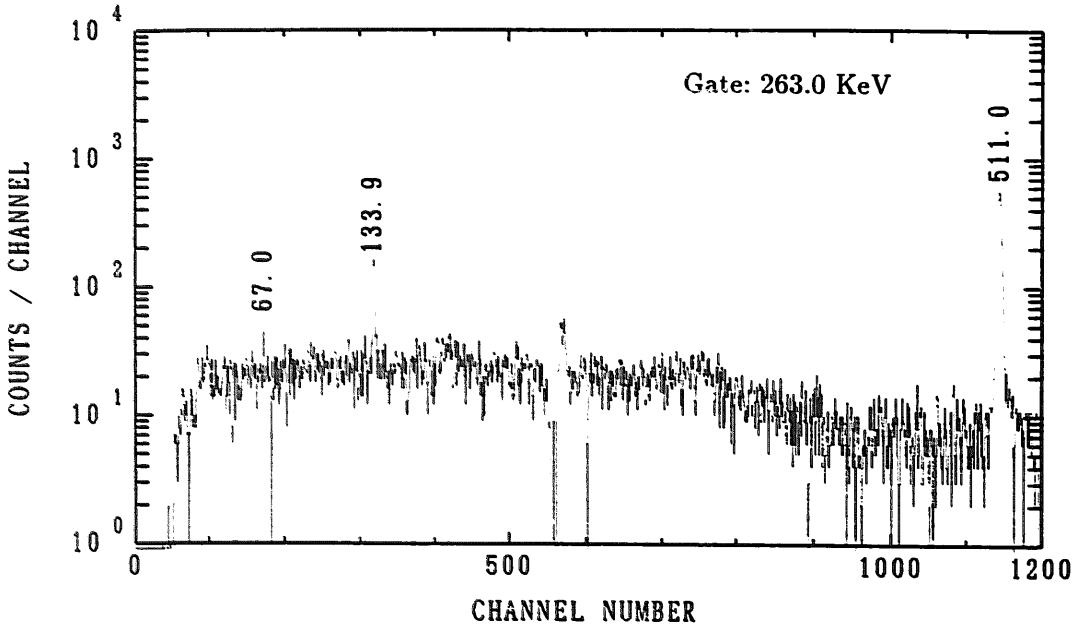


Fig. 3. Gamma-ray spectrum obtained in coincidence with the 263.0 keV $\gamma$-rays. The background has been subtracted.

intensities and half-lives of the $\gamma$-rays following the decay of $^{87}$Mo are summarized in table 1, together with values from previous works [2,3]).

*3.1.3. Measurement of internal conversion electrons.* Singles spectra of internal conversion electrons are shown in fig. 4. The K-conversion coefficients of the 135.0 and 201.0 keV transitions following the decay of $^{87}$Nb and the 263.0 keV transition following the decay of $^{87}$Mo were determined to be $2.02 \pm 0.12$, $0.049 \pm 0.005$ and $0.016 \pm 0.003$, respectively. Comparison between the experimental and theoretical values is shown in fig. 5. From this comparison multipolarities of the 135.0, 201.0 and 263.0 keV $\gamma$-rays were determined to be E3, M1+E2 and M1, respectively. These results are summarized in table 2.

TABLE 1

Gamma rays from the decay of $^{87}$Mo

| Energy (keV) | Present work | | Negra *et al.* | | Korshineck *et al.* | |
|---|---|---|---|---|---|---|
| | relative intensity (%) | $T_{1/2}$ (s) | relative intensity (%) | $T_{1/2}$ (s) | relative intensity (%) | $T_{1/2}$ (s) |
| 67.0 (3) | 0.7 (6) | - | - | - | - | - |
| 133.9 (1) | 6 (3) | 14.2 (10) | - | - | - | - |
| 263.0 (1) | 100 (1) | 14.3 (3) | 100 | 15 (2) | - | 14.1 (2) |
| 334.0 (4) | 4 (3) | - | - | - | - | - |
| 396.8 (1) | 37 (5) | 14.7 (5) | 38 | 15 (2) | - | 12.4 (5) |

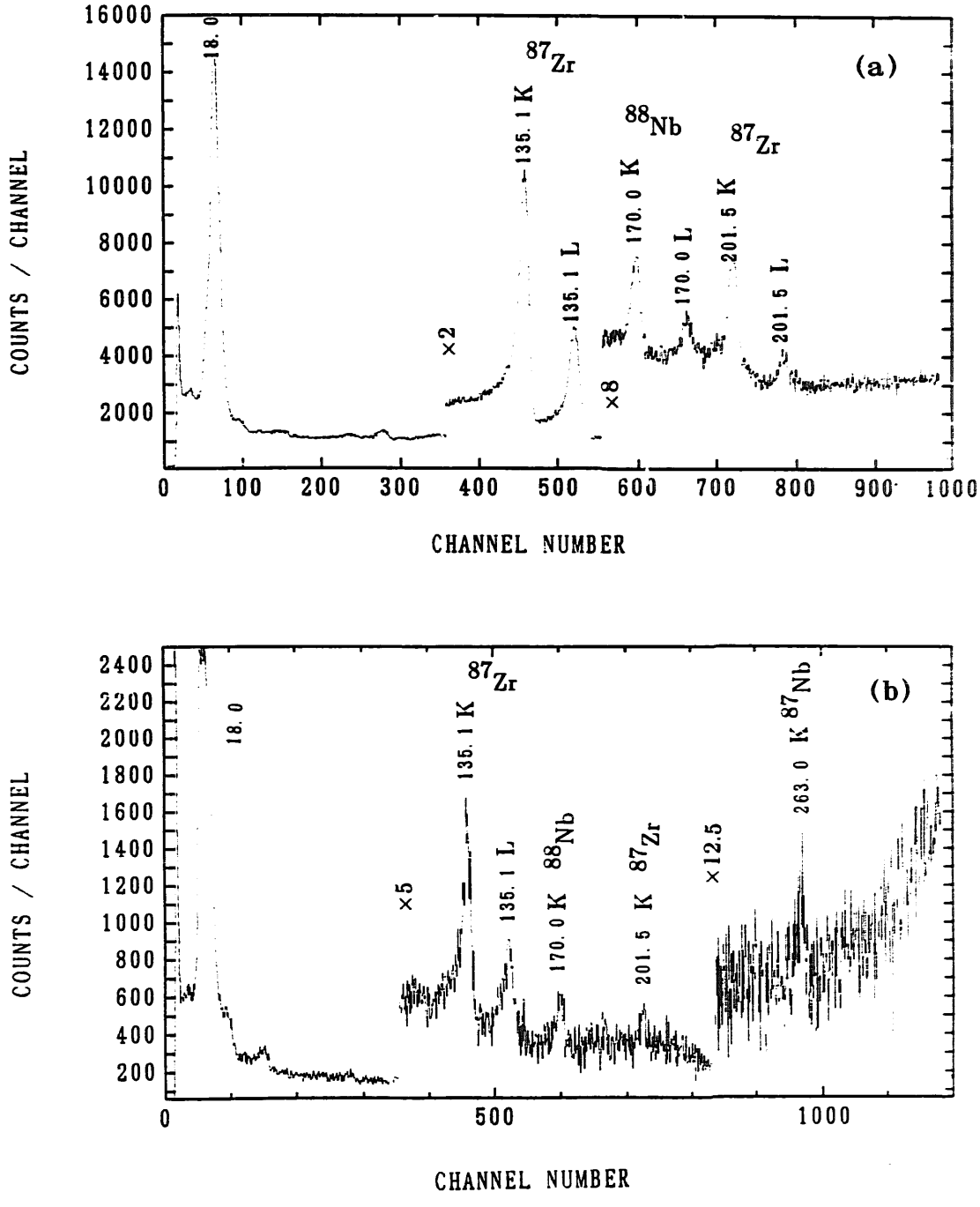


Fig. 4. Singles spectra of internal conversion electrons following the decay of $^{87}$Nb (a) and $^{87}$Mo (b). The irradiation and measurement times were selected 200 s for the $^{87}$Nb case and 10 s for the $^{87}$Mo case.

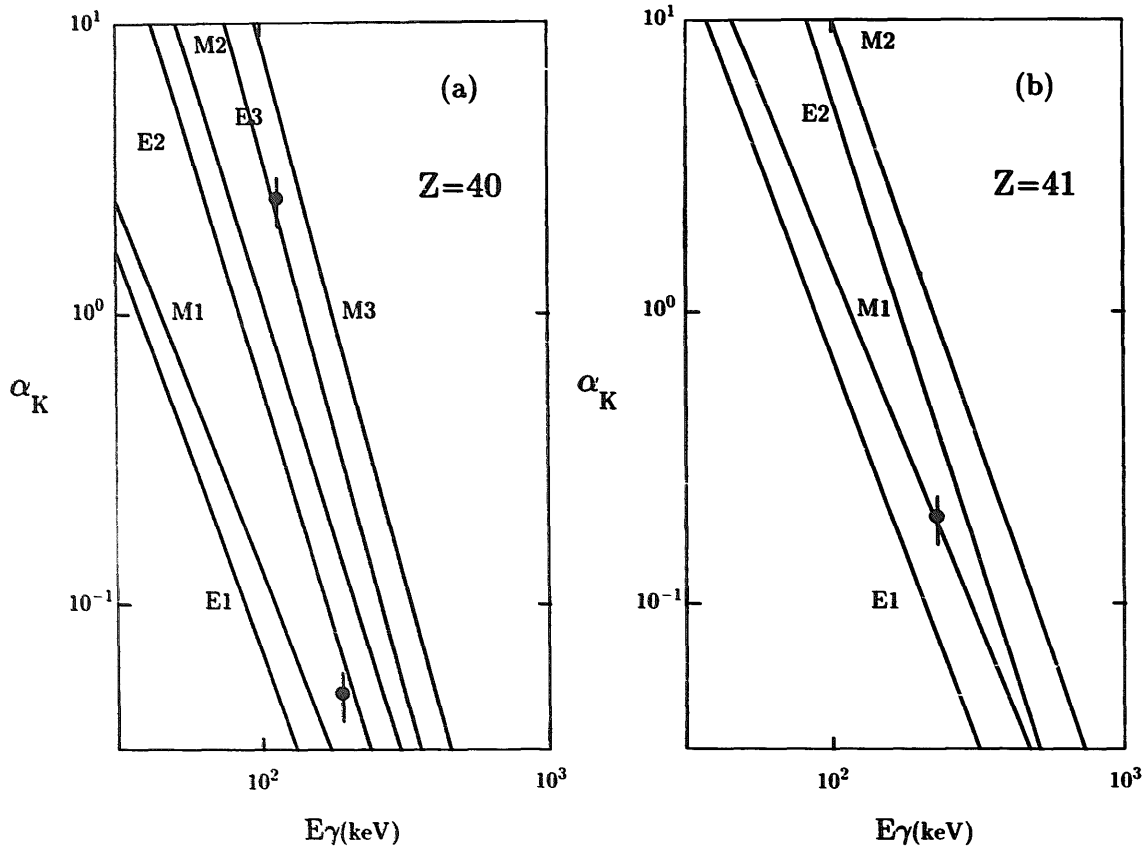


Fig. 5. Comparison between experimental and theoretical values of K-conversion coefficient for $Z = 40$ (a) and for $Z = 41$ (b).

### 3.2. IN-BEAM STUDY OF $^{87}Nb$

*3.2.1. Assignment of γ-rays.* Gamma-ray spectra from the $^{58}Ni(^{32}S, xp\gamma)$ reaction, gated by 1, 2, 3, and 4 protons are shown in fig. 6. Most of γ-rays in these spectra were firstly observed. The figure demonstrates clearly the channel selectivity of the particle-γ-coincidence technique.

Gamma rays from the 3pn and 4p, as well as 3p channel could be present in the 3p-gated spectrum. But the γ-rays from the 3pn and 4p reaction channels do not contaminate the 3p-gated spectrum because of the small cross section. From intensity

TABLE 2

Conversion coefficients for $^{87}Zr$ and $^{87}Nb$

| Energy (keV) | Conversion coefficient | | $K/(L+M)$ ratio | Mixing ratio | Multipolarity |
|---|---|---|---|---|---|
| | $K$-shell | $L+M$ shell | | | |
| $^{87}Zr$ 135.0 (1) | 2.02 (12) | 0.71 (6) | 3.02 (3) | - | E3 |
| 201.0 (5) | $4.9\,(5)\times10^{-2}$ | $7.3\,(7)\times10^{-3}$ | 7.07 (36) | 0.72 (10) | M1+E2 |
| $^{87}Nb$ 263.0 (4) | $1.6\,(3)\times10^{-2}$ | - | - | - | M1 |

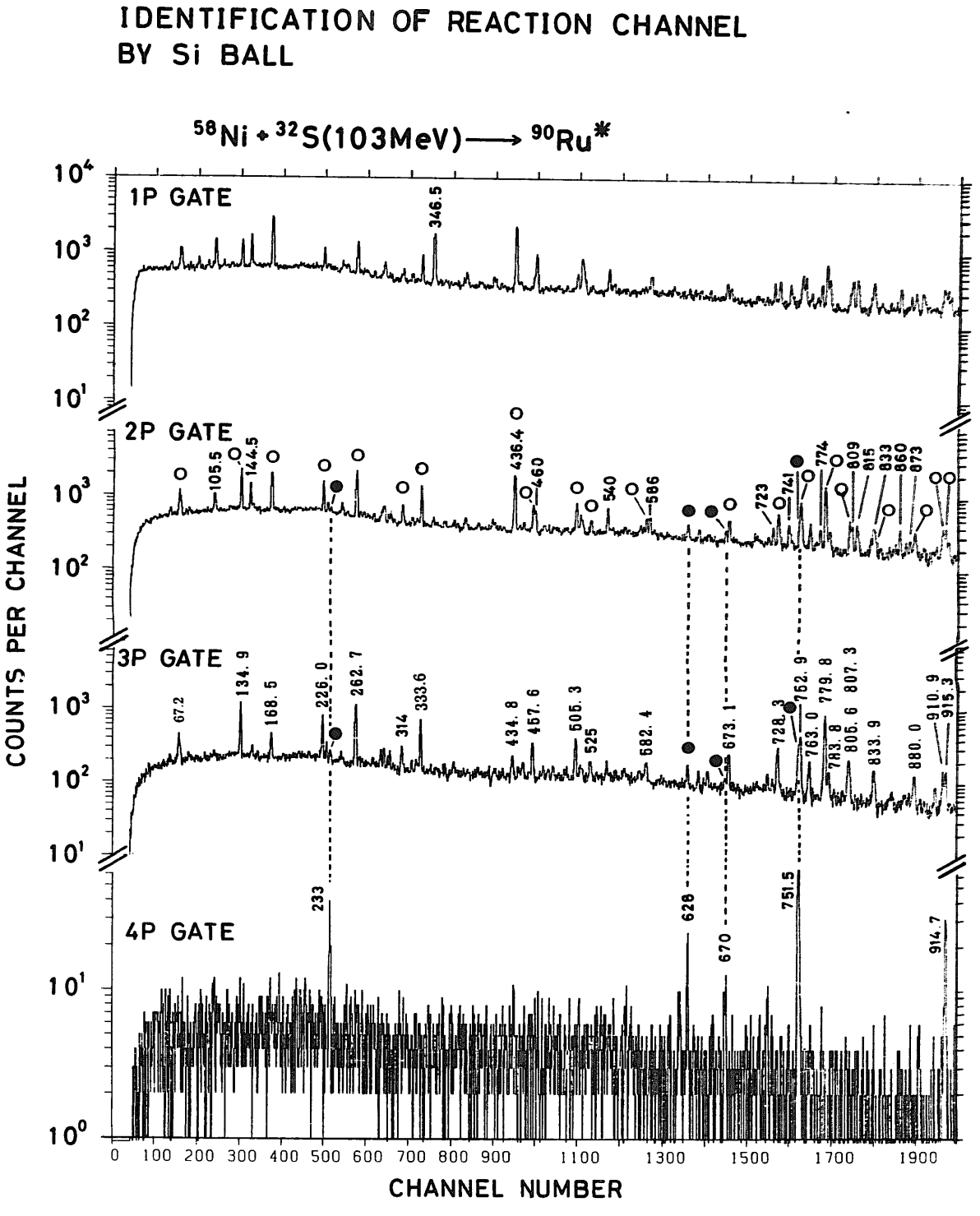


Fig. 6. Gamma-ray spectra following the $^{58}$Ni+$^{32}$S(103 MeV) reaction in coincidence with 1, 2, 3, and 4 proton(s). [open circle: $^{87}$Nb(3p) closed circle: $^{86}$Zr(4p)].

TABLE 3

Summary of gamma-ray energies, relative intensities and angular distributions for $^{87}$Nb

| $E_\gamma$ (keV) | Intensity (%) | $A_2$ | $A_4$ | Assignment |
|---|---|---|---|---|
| 67.2 | 1.7 (2) | - | - | $\frac{5}{2}^- \rightarrow \frac{7}{2}^+$ |
| 134.9 | 9.4 (2) | −0.27 (1) | 0.02 (2) | $\frac{17}{2}^- \rightarrow \frac{15}{2}^-$ |
| 168.5 | 4.0 (2) | 0.37 (3) | −0.02 (4) | |
| 226.0 | 11.3 (4) | −0.26 (1) | −0.03 (2) | $\frac{25}{2}^+ \rightarrow \frac{23}{2}^+$ |
| 230.5 | 2.7 (3) | - | - | |
| 262.7 | 23.1 (6) | −0.19 (3) | −0.05 (4) | $\frac{7}{2}^+ \rightarrow \frac{9}{2}^+$ |
| 290.5 | 2.2 (3) | - | - | $(\frac{29}{2}^+) \rightarrow (\frac{27}{2}^+)$ |
| 293.4 | 4.0 (3) | - | - | |
| 300.1 | 2.5 (3) | - | - | $\frac{15}{2}^- \rightarrow (\frac{13}{2}^-)$ |
| 313.1 | 4.7 (3) | - | - | |
| 333.6 | 23.0 (6) | 0.11 (6) | −0.03 (8) | $\frac{5}{2}^- \rightarrow \frac{1}{2}^-$ |
| 396.4 | 1.8 (4) | - | - | |
| 434.8 | 6.6 (4) | - | - | $\frac{11}{2}^- \rightarrow \frac{9}{2}^-$ |
| 446.9 | 2.7 (3) | - | - | |
| 457.6 | 12.9 (4) | - | - | $\frac{17}{2}^- \rightarrow \frac{15}{2}^+$ |
| 505.3 | 14.3 (8) | −0.52 (3) | 0.10 (5) | $\frac{7}{2}^- \rightarrow \frac{5}{2}^-$ |
| 521.6 | 3.8 (5) | −0.50 (5) | 0.03 (5) | $\frac{25}{2}^+ \rightarrow \frac{23}{2}^+$ |
| 558.7 | 1.0 (7) | - | - | $(\frac{27}{2}^+) \rightarrow \frac{25}{2}^+$ |
| 582.4 | 6.2 (24) | - | - | |
| 673.1 | 20.1 (7) | 0.45 (6) | −0.15 (7) | $\frac{15}{2}^- \rightarrow \frac{11}{2}^-$ |
| 675.0 | 2.8 (5) | - | - | |
| 728.3 | 17.1 (8) | −0.64 (9) | 0.17 (11) | $\frac{23}{2}^+ \rightarrow \frac{21}{2}^+$ |
| 752.9 | 48.6 (15) | 0.41 (2) | −0.17 (3) | $\frac{21}{2}^+ \rightarrow \frac{17}{2}^+$ |
| 763.0 | 18.7 (6) | 0.35 (8) | −0.10 (10) | $\frac{11}{2}^- \rightarrow \frac{7}{2}^-$ |
| 779.8 | 100.0 (11) | 0.37 (1) | −0.12 (2) | $\frac{13}{2}^+ \rightarrow \frac{9}{2}^+$ |
| 783.8 | 10.5 (8) | 0.28 (4) | −0.12 (5) | $\frac{11}{2}^+ \rightarrow \frac{7}{2}^+$ |
| 805.6 | 21.5 (12) | - | - | $\frac{21}{2}^- \rightarrow \frac{17}{2}^-$ |
| 807.3 | 11.0 (11) | - | - | $(\frac{13}{2}^-) \rightarrow \frac{9}{2}^-$ |
| 833.9 | 16.9 (8) | 0.36 (3) | −0.13 (4) | $\frac{9}{2}^- \rightarrow \frac{5}{2}^-$ |
| 854.3 | 1.2 (5) | - | - | $(\frac{27}{2}^+) \rightarrow \frac{25}{2}^+$ |
| 878.2 | 12.7 (24) | - | - | $\frac{29}{2}^- \rightarrow \frac{25}{2}^-$ |
| 880.0 | 5.7 (14) | - | - | $\frac{25}{2}^+ \rightarrow \frac{21}{2}^+$ |
| 902.1 | 6.9 (11) | 0.30 (2) | −0.05 (3) | $(\frac{15}{2}^+) \rightarrow \frac{11}{2}^+$ |
| 910.9 | 17.7 (32) | 0.37 (7) | −0.04 (10) | $\frac{25}{2}^- \rightarrow \frac{21}{2}^-$ |
| 951.5 | 75.1 (15) | 0.37 (4) | −0.10 (5) | $\frac{17}{2}^+ \rightarrow \frac{13}{2}^+$ |
| 954.3 | 11.0 (6) | 0.19 (5) | 0.03 (6) | $\frac{25}{2}^+ \rightarrow \frac{21}{2}^+$ |
| 958.0 | 6.6 (5) | - | - | |
| 1122.6 | 8.8 (6) | 0.25 (9) | 0.06 (6) | $\frac{21}{2}^+ \rightarrow \frac{17}{2}^+$ |
| 1144.5 | 10.0 (6) | - | - | $(\frac{29}{2}^+) \rightarrow \frac{25}{2}^+$ |
| 1168.3 | 4.1 (5) | - | - | $(\frac{15}{2}^+) \rightarrow \frac{13}{2}^+$ |
| 1248.1 | 4.5 (6) | - | - | $(\frac{33}{2}^+) \rightarrow (\frac{29}{2}^+)$ |
| 1376.1 | 7.0 (7) | - | - | |

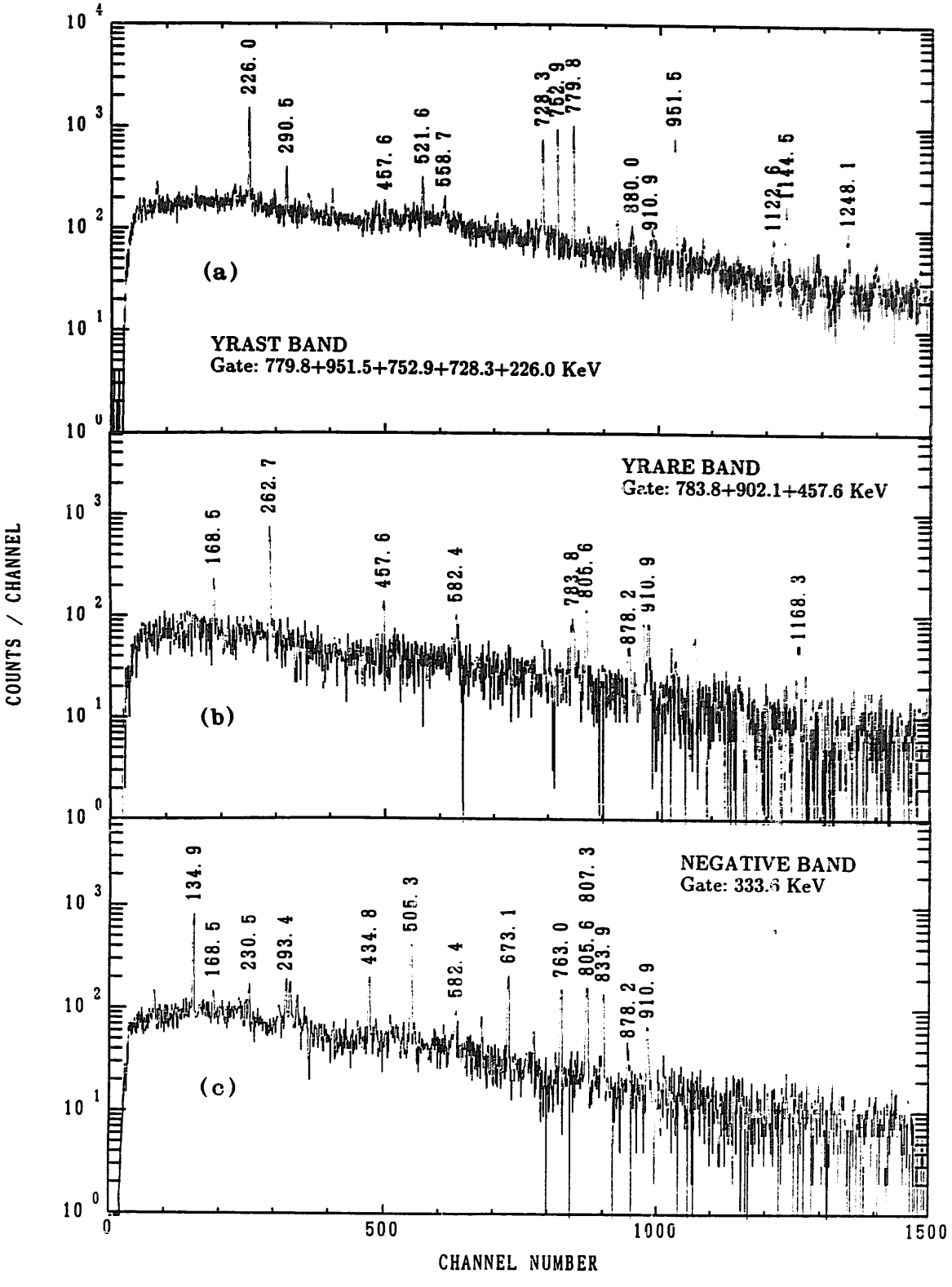


Fig. 7. Summed (charged particle) $\gamma\gamma$-coincidence spectra in the $^{58}$Ni($^{32}$S, 3p$\gamma$)$^{87}$Nb reaction at the beam energy of 103 MeV. Peaks are labelled by their energies in keV.

ratios [$I_\gamma$(3p)/$I_\gamma$(2p), $I_\gamma$(4p)/$I_\gamma$(3p)], where $I_\gamma(xp)$ is the $\gamma$-ray intensity in an $x$p-gated spectrum, it was found that the most of $\gamma$-rays in the 3p-gated spectrum belong to $^{87}$Nb. The energies and relative intensities of $\gamma$-rays assigned to $^{87}$Nb were obtained by the ($x$p) $\gamma$-coincidence experiment, which are summarized in table 3.

*3.2.2. (Charged particle)$\gamma\gamma$-coincidence measurement.* From careful consideration of the coincidence spectra, we find three distinct bands: yrast, yrare positive- and yrare negative-parity bands of which sequences start with 779.8, 262.7 and 333.6 keV transitions, respectively.

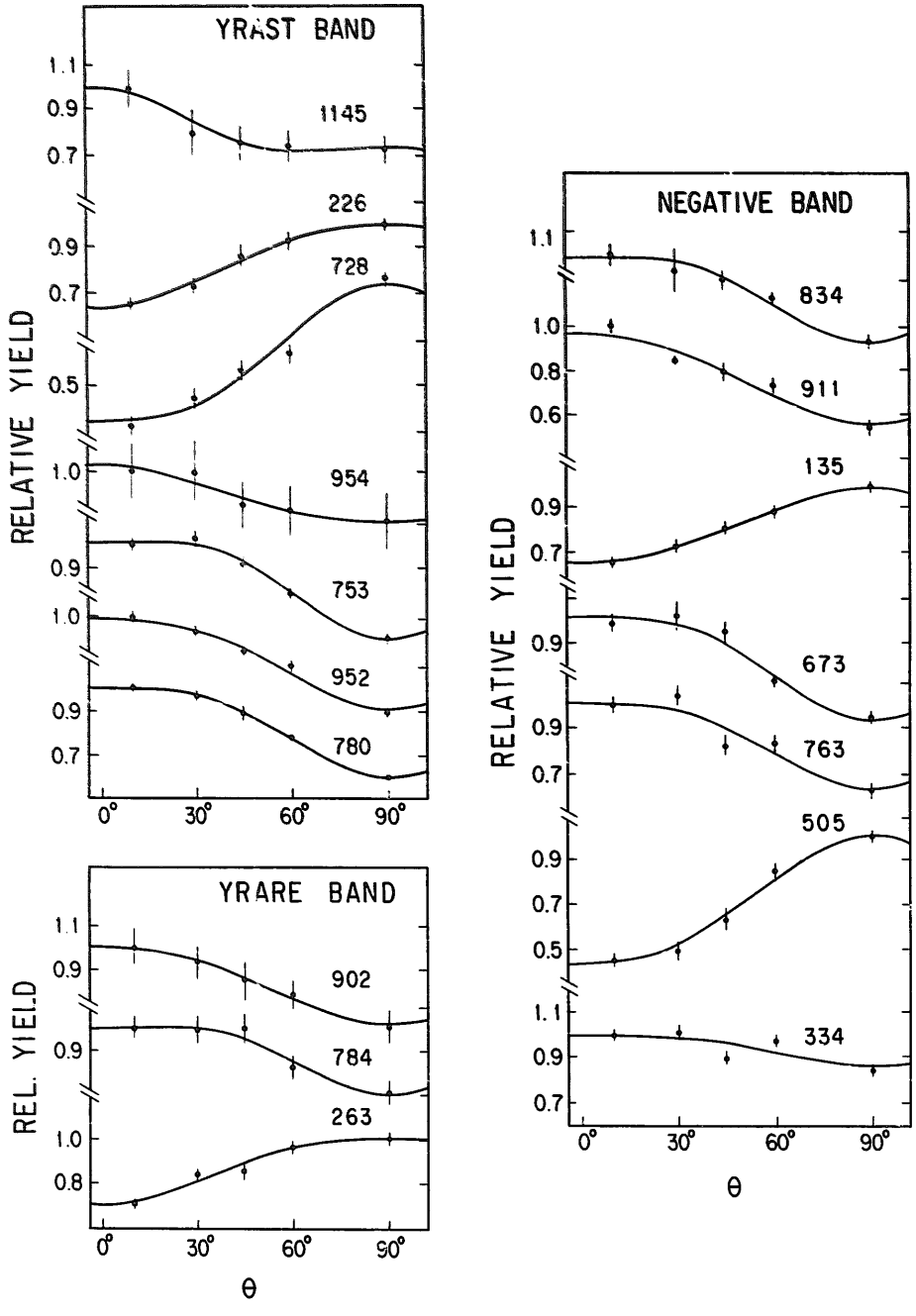


Fig. 8. Angular distribution of the $\gamma$-rays in $^{87}$Nb. The curves show fits by eq. (1).

To improve the statistical accuracy, spectra gated by $\gamma$-rays in a same cascade were summed. The results obtained by summing spectra gated by 226.0, 728.3, 752.9, 779.8 and 951.5 keV $\gamma$-rays and by the 783.8, 902.1 and 457.6 keV $\gamma$-rays are shown in fig. 7a, b. Fig 7c shows the spectrum gated by the 334.0 keV $\gamma$-ray.

*3.2.3. Angular distribution.* Results of angular-distribution measurements were fitted to the function defined by

$$W(\theta) = A_0(1 + A_2Q_2P_2(\cos\theta) + A_4Q_4P_4(\cos\theta)), \quad (1)$$

where $P_2$ and $P_4$ are the Legendre polynomials, and $Q_2$ and $Q_4$ are attenuation coefficients associated with finite solid angle of the detector. Fig. 8 shows the resulting fits, and the values of $A_2$ and $A_4$ for the $\gamma$-rays assigned to $^{87}$Nb are summarized in table 3.

## 4. Construction of level scheme

### 4.1. THE DECAY SCHEME OF $^{87}$Mo

To study the decay properties of $^{87}$Mo, assignment of the spins and parities to the low-lying states in $^{87}$Nb are important. However, $J^\pi$ assignment of these states are not definite as yet, because $J^\pi$ of the low-lying states of $^{87}$Zr are also not clarified. In the present work, the conversion electrons for low-lying transitions in $^{87}$Zr were measured and new informations are obtained. Thus, we discuss low-lying states in $^{87}$Zr, firstly.

*4.1.1. The $J^\pi$ of low-lying states in $^{87}$Zr.* The decay schemes of $^{87m,87}$Nb have been previously reported [1-3]) and low-lying parts of the schemes are shown in the upper part of fig. 9. But spins and parities of low-lying states in $^{87}$Zr have not been established. The ground state of $^{87}$Zr has been proposed [1]) to be $J^\pi = \frac{7}{2}^+$ or $\frac{9}{2}^+$. In the present experiment, multipolarities of the 135.0 and 201.0 keV $\gamma$-rays were determined to be E3 and M1 + E2, respectively.

From the multipolarities of the transitions, several candidates of spins and parities, for the 336.0, 201.0 keV and ground state, can be considered: $(\frac{11}{2}^-, \frac{5}{2}^+, \frac{7}{2}^+)$, $(\frac{1}{2}^-, \frac{7}{2}^+, \frac{7}{2}^+)$, $(\frac{3}{2}^-, \frac{9}{2}^+, \frac{7}{2}^+)$, $(\frac{1}{2}^-, \frac{7}{2}^+, \frac{9}{2}^+)$, $(\frac{3}{2}^-, \frac{9}{2}^+, \frac{9}{2}^+)$ and $(\frac{5}{2}^-, \frac{11}{2}^+, \frac{9}{2}^+)$.

The upper limit of the intensity ratio of the not-observed 336.0 keV $\gamma$-ray to the 135.0 keV $\gamma$-ray is estimated to be $4 \times 10^{-2}$ from the singles gamma-ray spectrum. This value leads to a partial half-life larger than $1.4 \times 10^3$ s for the 336.0 keV transition. Then, it is considered that E3 or M2 nature for 336 keV transition are not favoured because the half-lives by the Weisskopf estimate for E3 and M2 transitions are $5.4 \times 10^{-3}$ and $3.7 \times 10^{-7}$ s, respectively, which both give a too large transition strength. Besides, the half-life by the Weisskopf estimate with correction for internal conversion process for M4 transition is $3.4 \times 10^5$ s.

Taking into account that the 336 keV transition is a cross-over transition of E3 and M1 + E2 cascade, possible spin difference between ground and 336 keV states

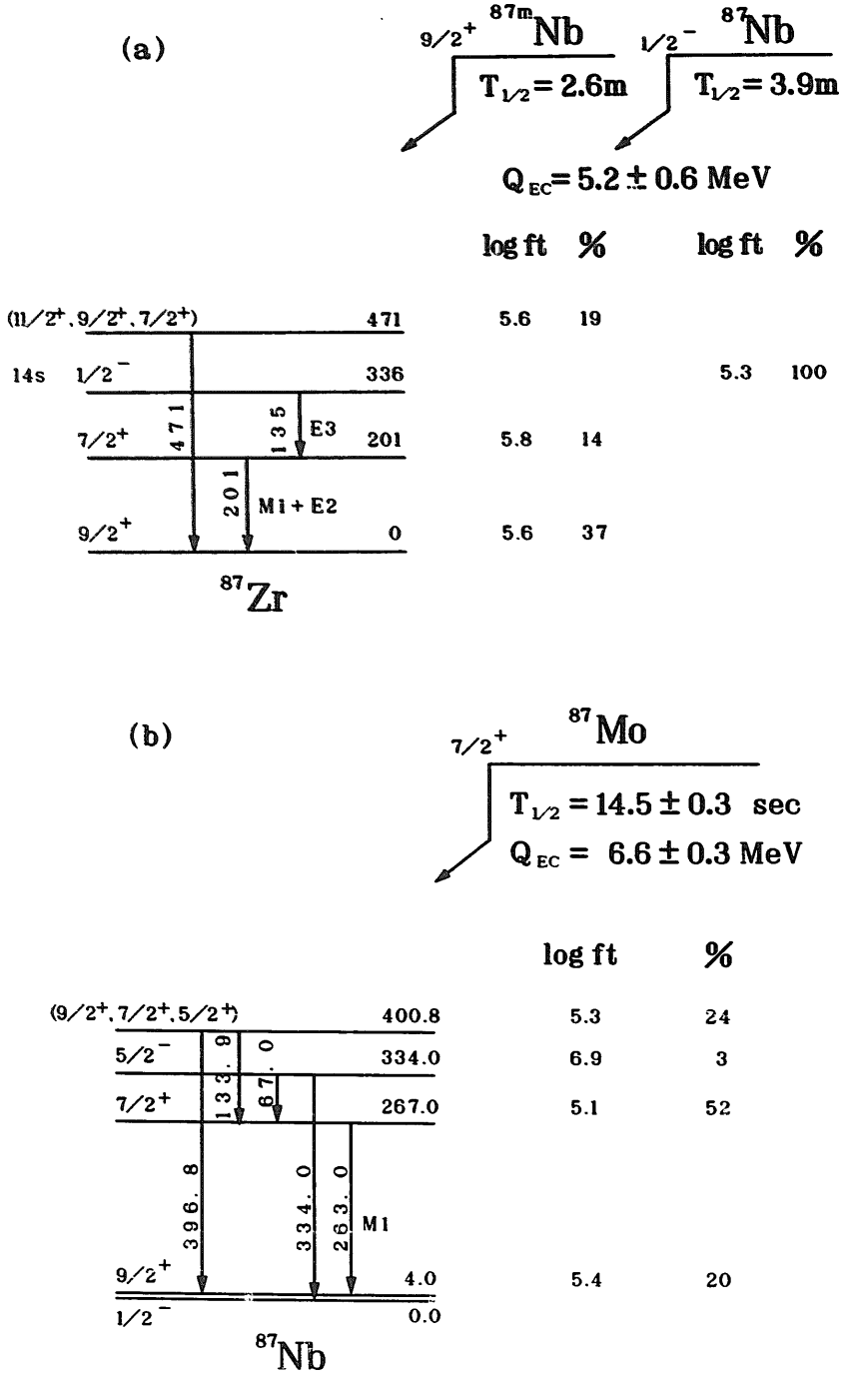


Fig. 9. The proposed decay schemes for $^{87}$Nb and $^{87}$Mo.

would be at least $4\hbar$. Thus $J^\pi$ of ($\frac{1}{2}^-$, $\frac{7}{2}^+$, $\frac{9}{2}^+$) candidate is assigned to the 336.0, 201.0 keV and ground states, respectively, in $^{87}$Zr (see fig. 9a).

On the other hand, systematical change of low-lying level structure in the $N=47$ isotones is shown in fig. 10 [ref. [9])]. In the nuclei of $^{85}$Sr, $^{87}$Zr and $^{89}$Mo, positions of the low-lying states ($\frac{1}{2}^-$, $\frac{7}{2}^+$ and $\frac{9}{2}^+$) change gradually in the same order of $J^\pi$. The present assignments of $J^\pi$ are natural in a viewpoint of the systematics, and are consistent with previous propositions [1,12]).

*4.1.2. $J^\pi$ assignment of low-lying states in $^{87}$Nb and $^{87}$Mo.* It has been proposed that the low-lying states of $^{87}$Nb consist of an isomeric pair of $\frac{1}{2}^-$ state with a half-life of 3.9 min and $\frac{9}{2}^+$ state with a half-life of 2.6 min [ref. [3])]. However, it has not been known which one is the ground state. To clarify that, we studied the $\beta$-decay of $^{87}$Mo by investigating which state (one of the isomeric pair) is populated by the 263.0 keV $\gamma$-ray following the decay of $^{87}$Mo.

If the 263.0 keV $\gamma$-ray populates the $\frac{9}{2}^+$ state of $^{87}$Nb, the 471.0 keV level (in $^{87}$Zr) is fed not only from $\beta$-decay of this $\frac{9}{2}^+$ state but also from 263.0 keV transition following the $\beta$-decay of $^{87}$Mo (see fig. 9). If the assumption is proper, the decay curve of the 471.0 keV $\gamma$-ray would have a growth portion, which should be associated with the initial yield of $^{87}$Mo. Therefore we made an analysis of the growth portion of the 471.0 keV $\gamma$-ray. The result showed that the 263.0 keV transition populates the $\frac{9}{2}^+$ state of $^{87}$Nb. But it has not been determined yet whether the ground state of $^{87}$Nb is a $\frac{9}{2}^+$ or a $\frac{1}{2}^-$ state, and that will be described below.

From the above mentioned result, the decay scheme of $^{87}$Mo (decays to the $\frac{9}{2}^+$ and its related states of $^{87}$Nb), as shown in fig. 9b, was firstly constructed. Since log $ft$ value for a $\beta$-branch to the 267.0 keV ($\frac{7}{2}^+$) state in $^{87}$Nb is 5.1, assignment of $J^\pi = \frac{5}{2}^+$, $\frac{7}{2}^+$ or $\frac{9}{2}^+$ for the ground state of $^{87}$Mo is possible. Assignment of $\frac{7}{2}^+$ to the 267.0 keV level is probable, and it is proven by analysis of the in-beam data. The 400.8 keV level was tentatively assigned to be $J^\pi = \frac{9}{2}^+$, $\frac{7}{2}^+$ or $\frac{5}{2}^+$. Since the 334.0 keV

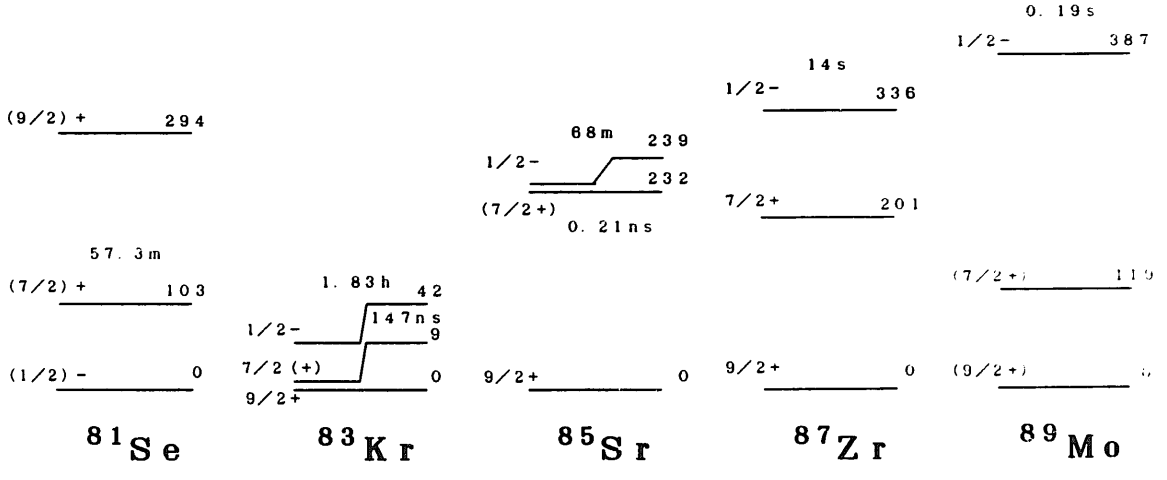


Fig. 10. Systematics of $N=47$ isotones.

level was strongly fed in in-beam measurements, an assignment of $J^{\pi}$ to this level are discussed in the following section.

### 4.2. THE LEVEL SCHEME OF $^{87}$Nb

Based on the results of present experiments, decay scheme of the excited levels of $^{87}$Nb is proposed, as shown in fig. 11, and consists of three bands corresponding to the three groups in the $\gamma\gamma$-coincidence results.

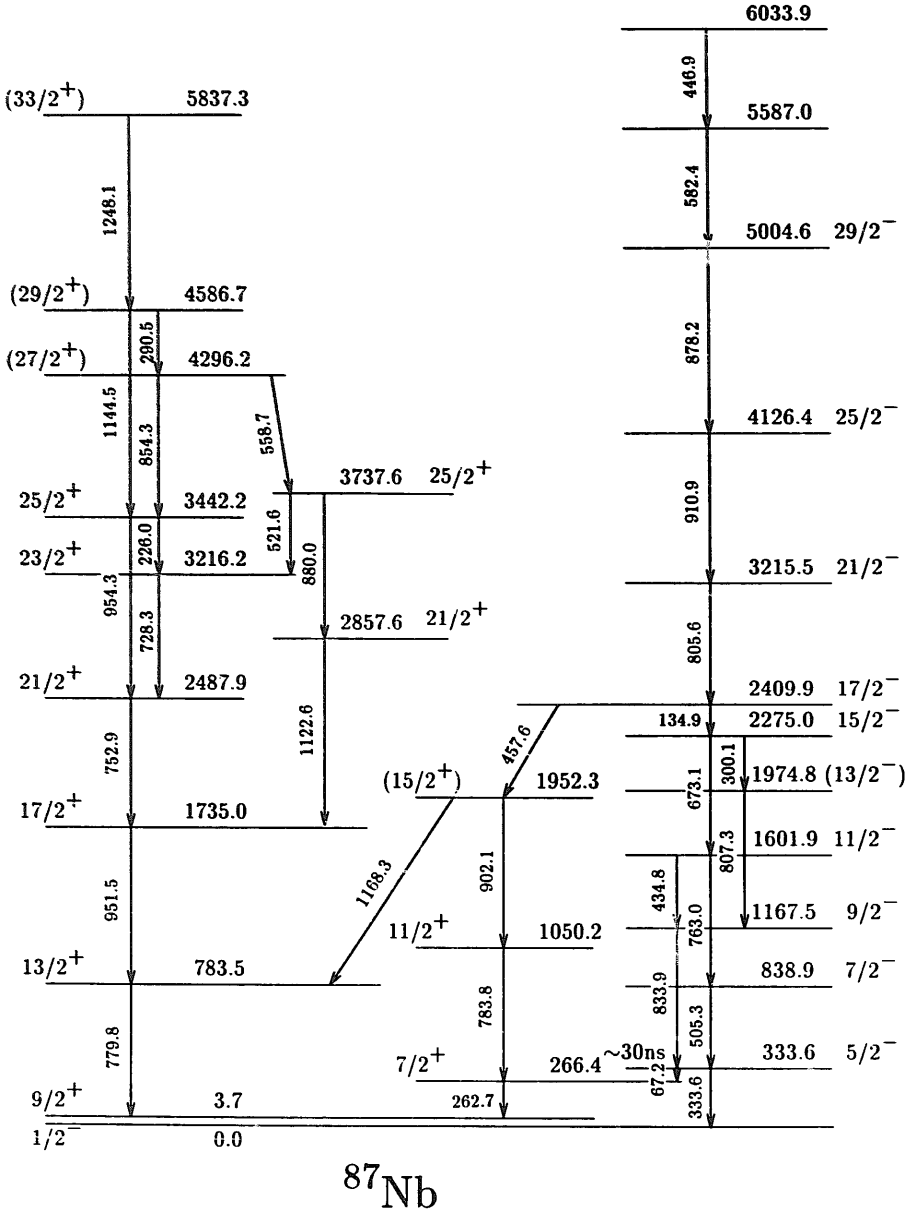


Fig. 11. Proposed level scheme of $^{87}$Nb. The position of the $\frac{9}{2}^{+}$ isomeric state at 3.7 keV has been confirmed in association with the decay study of $^{87}$Mo.

*4.2.1. Low-lying levels.* From the in-beam $\gamma\gamma$-coincidence measurement, it was found that the 262.7 keV $\gamma$-ray is strongly in coincidence with 67.2 keV $\gamma$-ray but not with 333.6 keV $\gamma$-ray. The 333.6 keV $\gamma$-ray is not in coincidence with the 67.2 and 262.7 keV $\gamma$-rays. Moreover, these three $\gamma$-rays are in coincidence with the 505.3 keV $\gamma$-ray. The energy difference betwen the 333.6 keV $\gamma$-ray and the energy sum of the 67.2 and 262.7 keV $\gamma$-rays is 3.7 keV. The energy sum of the 779.8 and 1168.3 keV $\gamma$-rays cascade and of the 262.7, 783.8 and 902.1 keV $\gamma$-rays cascade have the same value and these $\gamma$-rays are also in coincidence with the 457.6 keV $\gamma$-ray. Considering the above result, the low-lying part of the level scheme can be constructed as shown in fig. 11. This result does not contradict with the level scheme (fig. 9b) of $^{87}$Nb obtained from the $^{87}$Mo decay, and it is concluded that the $\frac{1}{2}^-$ ground state of $^{87}$Nb is 3.7 keV lower than the $\frac{9}{2}^+$ state.

*4.2.2. $J^\pi$ assignment.* On the basis of the multipolarities of the deexcitation $\gamma$-rays, spins and parities of the excited states of $^{87}$Nb were assigned. We assume, in this section, dipole and quadrupole to be of M1 and E2 nature, respectively.

*The positive-parity band.* In the yrast band, the 779.8, 951.5 and 752.9 keV transitions are pure E2 transitions, so the transitions are assigned to $\frac{13}{2}^+ \rightarrow \frac{9}{2}^+$, $\frac{17}{2}^+ \rightarrow \frac{13}{2}^+$ and $\frac{21}{2}^+ \rightarrow \frac{17}{2}^+$, respectively. The M1 transitions of 728.3 and 226.0 keV are assigned to $\frac{23}{2}^+ \rightarrow \frac{21}{2}^+$ and $\frac{25}{2}^+ \rightarrow \frac{23}{2}^+$, respectively. These assignments are supported by the E2 character of the cross-over transition of 954.3 keV. The level at 4586.7 keV is assigned to be $J^\pi = (\frac{29}{2}^+)$, when the trend of the angular distribution of the 1144.5 keV $\gamma$-ray is considered. The 5837.3 keV level can be speculated to be $(\frac{33}{2}^+)$ because of the systematical behavior of transition energy in this band.

Spins of the positive-parity yrare levels at 266.4, 1050.2 and 1952.3 keV are assigned to $\frac{7}{2}^+$, $\frac{11}{2}^+$ and $(\frac{15}{2}^+)$, respectively, because the transitions of 783.8 and 902.1 keV are pure E2.

The 262.7 keV transition was refitted to the expression of eq. (1) with a free parameter of mixing ratio $\delta$ for each choice of initial spin $J_i$, using the formalism of Yamazaki [13]). In the formalism, $A_k(k=4)$ in eq. (1) is expressed by the following form: $A_k = \alpha_k / A_k^{\max}$, where $A_k^{\max}$ is a known function of $J_i$, $J_j$ and $\delta$, and $\alpha_k$ is an attenuation coefficient of alignment. The values of $\alpha_2$ for the $\frac{11}{2}^+$ state is deduced to be 0.62 from analysis of the 783.8 keV transition. Therefore, $\alpha_2 = 0.62$ was used for the 262.7 keV transition. The $\alpha_4$ coefficient was calculated by assuming a gaussian distribution of the magnetic substate [13]), and turned out to be 0.24. At the $\chi^2$ minimum, the transition has a small quadrupole admixture ($\delta = 0.12$).

*The negative-parity band.* The transitions of 833.9, 763.0, 673.1 and 910.9 keV have the pure E2 characteristics, and the 505.3 and 134.9 keV transitions show an angular distribution of M1 type. Because of the small energy difference between the 805.6 and 807.3 keV $\gamma$-rays, their multipolarities of the $\gamma$-rays were not assigned exactly. However, they have a tendency of the E2 characteristic. The characteristic of the 333.6 keV transition was decided to be E2, next spin and parity of this level was

determined to be $\frac{5}{2}^-$. Hence, in this band, the spins and parities of the states up to 5004.6 keV are assigned as shown in fig. 11.

## 5. Discussion

### 5.1. THE LOW-LYING STATES OF $^{87}$Nb POPULATED BY $\beta$-DECAY OF $^{87}$Mo

It has been known that the low-lying states of odd isotopes of Nb consist of $\frac{1}{2}^-$ and $\frac{9}{2}^+$ isomers. Non-uniform change of relative positions of these two states arised from change in nuclear structure from spherical to deformed shape. In the $^{91}$Nb and $^{89}$Nb nuclei [14,15]), $J^\pi$ of ground and first excited states are $\frac{9}{2}^+$ and $\frac{1}{2}^-$, respectively, but the ordering of the $J^\pi$ is reversed in $^{87}$Nb, as confirmed by the present experiment.

On the other hand, the ground-state spin of $^{87}$Mo is ambiguous ($\frac{5}{2}$, $\frac{7}{2}$ or $\frac{9}{2}$) in the present experiment. However, spins and parities of the ground states of $N=45$ isotones, i.e. from $^{81}$Kr to $^{85}$Zr, have been known to be $\frac{7}{2}^+$ without any exception [16,17]). The log $ft$ values for the $\beta$-transition from the ground state of $^{87}$Mo to the first excited state of $^{87}$Nb is 5.4. Accordingly, we proposed $J^\pi = \frac{7}{2}^+$ for the ground state of $^{87}$Mo. Moreover, the log $ft$ value of 6.9 for the 334.0 keV level in $^{87}$Nb supports this $\frac{7}{2}^+$ assignment to the ground state of $^{87}$Mo.

### 5.2. THE HIGH-SPIN STATES OF $^{87}$Nb

The limited information on Nb isotopes makes it difficult to discuss systematic behavior of nuclear structure of the isotopes. We present a discussion of the level structure of $^{87}$Nb mainly based on the in-beam experiment and the structure of $^{87}$Nb is compared to that of $^{85}$Y. The yrast band in these nuclei is very similar, but the negative-parity band is not.

The positive signature, $\alpha = +\frac{1}{2}$ yrast sequence of the positive-parity band was observed from the $\frac{9}{2}^+$ band head to the $(\frac{33}{2}^+)$ state in the present study. This sequence can be identified with the favored (f) signature sector of the decoupled proton $g_{9/2}$ band that has been observed systematically in the neighboring nuclei [5,18]). As shown in fig. 12, a backbending at $\hbar\omega = 0.45$ MeV characterizes this band in $^{87}$Nb. The studies on $^{83,85}$Y [refs. [18,5])] have clarified that this band is comparatively rotation-like before the backbending, whereas the collectivity becomes less after it.

In the unfavoured (u) signature sector ($\alpha = -\frac{1}{2}$), six states, $\frac{7}{2}^+$, $\frac{11}{2}^+$, $(\frac{15}{2}^+)$, $\frac{23}{2}^+_{(1)}$, $\frac{23}{2}^+_{(2)}$ and $(\frac{27}{2}^+)$ have been observed. A $\frac{7}{2}^+$-$\frac{11}{2}^+$-$(\frac{15}{2}^+)$ sequence among them may be regarded as the signature-partner sequence of the favored single-quasiparticle (1qp) sequence, $\frac{9}{2}^+$-$\frac{13}{2}^+$-$\frac{17}{2}^+$. The signature splitting $\Delta e'$ between these sequences can be calculated after transforming the observed energies of $\frac{9}{2}^+$-$\frac{13}{2}^+$-$\frac{17}{2}^+$ and $\frac{7}{2}^+$-$\frac{11}{2}^+$-$(\frac{15}{2}^+)$ into a rotating frame of reference by means of the standard technique [19]). The resulting value is $\Delta e' = 0.69$ MeV at $\hbar\omega = 0.4$ MeV. The large magnitude of $\Delta e'$, as well as the small

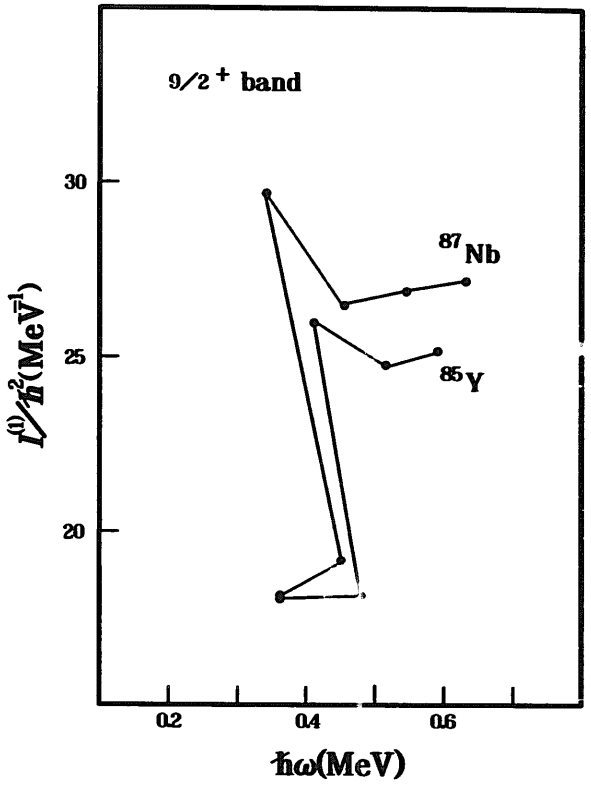


Fig. 12. Kinematical moment of inertia $I^{(1)}/\hbar^2$ of the yrast bands in $^{87}$Nb (present work) and $^{85}$Y [ref. [5])].

$B$(E2) values for the core nucleus $^{86}$Zr [ref. [20])], indicates that the quadrupole deformation is not well developed in $^{87}$Nb. Therefore, large amplitude fluctuations around small $\beta$ should be taken into account in describing the structure of the $g_{9/2}$ 1qp band in $^{87}$Nb.

Further evidence of the softness can be extracted from the sign of the E2/M1 mixing ratio $\delta$ associated with the $\Delta I = 1$ transitions between signature partners. It has been shown in ref. [21]) that the coupling with the small-amplitude gamma vibrations changes the sign of $\delta(I_f \to (I-1)_u)$ $[=-\delta((I-1)_u \to I_f)]$ given by the cranking model when the odd quasiparticle was decoupled from the deformed core. We expect that the coupling with large-amplitude quadrupole vibrations brings effects stronger than that of the small-amplitude modes. In fact, positive values of $\delta(\frac{7}{2}^+ \to \frac{9}{2}^+)$ were observed systematically in $^{87}$Nb (present work) and $^{83,85}$Y [refs. [18,5])]: it is contrary to the cranking model prediction for $\beta > 0$ and $\Delta e' > \hbar\omega$ [refs. [22,21])] because $g_j - g_k$ is positive for $\pi g_{9/2}$, and then we can regard the observed sign of $\delta(\frac{7}{2}^+ \to \frac{9}{2}^+)$ as evidence for the softness. Note that here we assume small but positive $\beta$'s for $^{87}$Nb and $^{85}$Y (referring to the $^{83}$Y case [18])).

The ground state is assigned to be $J^\pi = \frac{1}{2}^-$, but the negative-parity high-spin states show a complex structure, which is not exhibited in $^{85}$Y. Cascades feeding the $\frac{1}{2}^-$ ground state and 266 keV $\frac{5}{2}^-$ single-particle state [23]) have not been observed in $^{85}$Y. But cascades feeding the $\frac{1}{2}^-$ ground state and 333.6 keV $\frac{5}{2}^-$ state have been observed

in $^{87}$Nb. In particular, the 333.6 keV level has a half-life of ~30 ns which is almost same order of the Weisskopf single-particle estimate for E2 transition. This result points behavior of single particle in the lower part of negative-parity states.

## 6. Conclusion

The present work on low-lying states of $^{87}$Nb fed by $^{87}$Mo has established 4 new states and deduced log$ft$ values and definite, or very appropriate, spin-parity assignments. High-spin states of $^{87}$Nb were investigated and twenty-seven new states and $J^{\pi}$ assignments for many of them were established from the in-beam measurement. It was shown that the $^{87}$Nb nucleus has the interplay between collective- and independent-particle excitations.

We would like to thank Mr. T. Maeda for preparation of the electronic circuits and also Mr. Y. Koga for making the experimental apparatus. One of the authors (M.M.) is indebted to Fellowships of the Japan Society for the Promotion of Science for Japanese Junior Scientists.

## References

1) R. Turcotte, R. Iafigliola, R.B. Moore and J.K.P. Lee, Nucl. Phys. **A198** (1972) 67
2) G. Korschinek, E. Nolte, H. Hick, K. Miyano, W. Kutschera and H. Morinaga, Z. Phys. **A281** (1977) 409
3) S. Della Negra, D. Jacquet and Y. Le Beyec, Z. Phys. **A308** (1982) 243
4) E. Hagberg, J.C. Hardy, H. Schmeing, E.T.H. Clifford and V.T. Koslowsky, Nucl. Phys. **A395** (1983) 152
5) R. Diller, K.P. Lieb, L. Luhmann, T. Osipowicz, P. Sona, B. Wormann, L. Cleemann and J. Eberth, Z. Phys. **A321** (1985) 659
6) K. Heiguchi, T. Maeda, H. Tomura, B.J. Min, Y. Haruta, S. Mitarai and T. Kuroyanagi, Kyushu University Tandem Accelerator Laboratory Report KUTL REPORT-2 (1985-1987) 33
7) J. Mukai, R. Nakatani, B.J. Min, T. Maeda, S. Mitarai and T. Kuroyanagi, Gensikaku kenkyu, ISSN, vol. 33, No. 6 (1989) 219;
S. Mitarai, S. Suematsu, B.J. Min, H. Tomura, A. Nakatani, J. Mukai, T. Kuroyanagi, T. Morikawa, T. Komatsubara, S. Juutinen, J. Nyberg, D. Jerrestam, S.E. Arnell, Halina A. Roth and Ö. Skeppstedt, Report of the Research Meeting on gamma rays and nuclear structure, RCNP, Osaka, Japan, 31 Aug-2 Sept. RCNP-P-108 (1989) 20
8) T.A. Doron and M. Blann, Nucl. Phys. **A161** (1971) 12
9) Table of isotopes, 7th edition ed. C.M. Lederer and V.S. Shirley (Wiley, New York, 1978)
10) S. Della Negra, H. Gauvin, D. Jacquet and Y. Le Beyec, Z. Phys. **A307** (1982) 305
11) B.J. Min, S. Mitarai and T. Kuroyanagi, Kyushu University Tandem Accelerator Laboratory Report KUTL REPORT-2 (1985-1987) 124
12) J.E. Kitching, P.A. Batay-Csorba, C.A. Fields, R.A. Ristinen and B.L. Smith, Nucl. Phys. **A302** (1978) 159
13) T. Yamazaki, At. Data Nucl. Data Tables, 3 (1967) 1
14) K. Oxorn, S.K. Mark, J.E. Kitching and S.S.M. Wong, Z. Phys. **A321** (1985) 485
15) B.J. Diana, F.W.N. de Boer and C.A. Fields, Z. Phys. **A306** (1982) 171
16) L. Funke, J. Döring, P. Kemnitz, E. Will and G. Winter, Nucl. Phys. **A455** (1986) 206
17) S.E. Arnell, S. Sjöberg, Ö. Skeppstedt, E. Wallander, A. Nilsson and G. Finnas, Nucl. Phys. **A455** (1986) 206

18) C.J. Lister, B.J. Varley, W. Fieber, J. Heese, K.P. Liep, E.K. Warburton and J.W. Olness, Z. Phys. A329 (1988) 413
19) R. Bengtsson and S. Frauendorf, Nucl. Phys. A327 (1979) 139
20) E.K. Warburton, C.J. Lister, J.W. Olness, P.E. Haustein, S.K. Saha, D.E. Alburger, J.A. Becker, R.A. Dewberry and R.A. Naumann, Phys. Rev. C31 (1985) 1211
21) M. Matsuzaki, Nucl. Phys. A519 (1990) 548
22) G.B. Hagemann and I. Hamamoto, Phys. Rev. C40 (1989) 2862
23) L.R. Medsker, G.S. Florey, H.T. Fortune and R.M. Wieland, Phys. Rev. C12 (1975) 1452